

# Beam Test Performance of AstroPix sensor with 120 GeV protons

Bobae Kim<sup>a</sup>, Regina Caputo<sup>b</sup>, Manoj Jadhav<sup>a</sup>, Sylvester Joosten<sup>a</sup>, Carolyn Kierans<sup>b</sup>, Henry Klest<sup>a</sup>, Adrien Laviron<sup>b,c</sup>, Richard Leys<sup>d</sup>, Jessica Metcalfe<sup>a</sup>, Jared Richards<sup>a</sup>, Nicolas Striebig<sup>d</sup>, Amanda L. Steinhebel<sup>e</sup>, Daniel Violette<sup>b,c</sup>, Maria Žurek<sup>a</sup>

<sup>a</sup>Argonne National Laboratory, 9700 S. Cass Avenue, Lemont, IL 60439, Illinois, U.S.A.

<sup>b</sup>NASA Goddard Space Flight Center, 8800 Greenbelt Rd, Greenbelt, MD 20771, Maryland, U.S.A.

<sup>c</sup>NASA Postdoctoral Program Fellow (ORAU)

<sup>d</sup>ASIC and Detector Laboratory, Karlsruhe Institute of Technology, Hermann-von-Helmholtz-Platz 1, Karlsruhe, D-76344, Baden-Württemberg, Germany

<sup>e</sup>Oak Ridge National Laboratory, 1 Bethel Valley Road Oak Ridge, Oak Ridge, TN 37830, Tennessee, U.S.A.

## Abstract

AstroPix is a high-voltage CMOS (HV-CMOS) monolithic active pixel sensor (MAPS) developed for precision gamma-ray imaging and spectroscopy in the medium-energy regime, as well as for precise shower imaging and tracking in the Barrel Imaging Calorimeter (BIC) of the Electron Proton/Ion Collider (ePIC) detector at the future Electron-Ion Collider (EIC). We present beam test results of the AstroPix\_v3 sensor using a 120 GeV proton beam at the Fermilab Test Beam Facility (FTBF), performed as part of the broader experimental campaign for the BIC prototype calorimeter. The sensor's 500  $\mu\text{m}$  pixel pitch enabled precise measurement of the beam profile, providing important information for the calorimeter performance studies. Using the measured 120 GeV proton data, we measure the energy deposit of minimum ionizing particles and use them to extract the corresponding effective depletion depth.

**Keywords:** HV-CMOS MAPS, AstroPix, MIP response, depletion depth, Barrel Imaging Calorimeter, ePIC detector, EIC

## 1. Introduction

AstroPix has been developed for the proposed All-sky Medium-Energy Gamma-ray Observatory eXplorer (AMEGO-X) mission [1], a next-generation MeV gamma-ray telescope building on the heritage of Fermi Large Area Telescope (Fermi-LAT) [2]. AMEGO-X is designed to explore key questions in high-energy astrophysics, including the origins of cosmic rays and neutrinos, the physics of relativistic jets from neutron star mergers, the role of supermassive black holes, and the acceleration sites of galactic particles, while providing continuous full-sky monitoring of energetic transients. AMEGO-X is composed of a tracker, based on AstroPix, and a cesium iodide calorimeter. The AstroPix-based tracker is undergoing performance evaluation and technology validation through near-space and sub-orbital flight demonstrations, including the Compton and pair (ComPair-2) gamma-ray telescope [3] and the

AstroPix Sounding Rocket Technology dEmonstration Payload (A-STEP) [4].

In addition, AstroPix has been selected as the imaging layer for the Barrel Imaging Calorimeter (BIC) of the Electron Proton/Ion Collider (ePIC) detector at the future Electron-Ion Collider (EIC). The EIC will provide high-luminosity polarized electron–proton and electron–ion collisions with unprecedented precision. The ePIC experiment, the first experiment at the EIC, is dedicated to exploring fundamental questions in nuclear physics including the origin of the nucleon mass and the nucleon spin, as well as dense gluonic systems [5–7].

The BIC is the electromagnetic calorimeter in the barrel region of the ePIC detector and identifies scattered electrons, a key requirement for accurate reconstruction of event kinematics. The BIC consists of lead/scintillating-fiber (Pb/SciFi) sampling calorimeter layers interleaved with AstroPix-based imaging layers embedded in the front half of the calorimeter [8]. This structure provides precise three-dimensional imaging of particle showers, enabling essential performance capabilities such as  $e^-/\pi^\pm$  and  $\gamma/\pi^0$  separation, which are

\*Corresponding author

Email address: bobae.kim@anl.gov (Bobae Kim)

crucial for Deep Inelastic Scattering (DIS) measurements and for achieving the EIC’s scientific goals [7].

For the AstroPix imaging layers, one of the key requirements for the BIC is to achieve sufficient dynamic range to detect minimum ionizing particle (MIP) signals in all layers. The dynamic range and energy resolution of the third iteration of the AstroPix chips, AstroPix\_v3, have been studied using radioactive gamma-ray sources in a previous study [9]. Since 120 GeV protons behave as minimum ionizing particles, they provide an ideal beam to study the MIP response of AstroPix.

In this work, we extend these studies to a beam environment by testing AstroPix\_v3 with a 120 GeV proton beam at the Fermilab Test Beam Facility (FTBF) [10]. From 120 GeV proton data, we measure the energy deposited in the sensor and derive the corresponding effective depletion depth, which is a key parameter for accurate detector simulations and system-level performance studies. Section 2 describes the specifications of AstroPix\_v3 (Section 2.1), the beam-test preparation and calibration (Section 2.2), and the experimental setup used in the FTBF test (Section 2.3). Section 3 presents the beam test results, and Section 4 summarizes the conclusions and future prospects.

## 2. Experimental Setup

### 2.1. AstroPix\_v3

AstroPix is a novel high-voltage CMOS monolithic active pixel sensor (HV-CMOS MAPS) that benefits from a deep depletion region enabled by a high bias voltage, allowing fast drift-based charge collection and improved radiation hardness compared to conventional MAPS [11]. It features in-pixel amplification and in-pixel signal processing, as well as on-chip digitization, which minimizes signal routing and power consumption. Furthermore, the detector chips can be daisy-chained to enable efficient scalability to large-area and multilayer detectors.

Since 2019, the development and testing of AstroPix has progressed through several design iterations, from version 1 to version 4 [9, 12–17]. The on-going AstroPix Research and Development (R&D) aims to meet the requirements of both AMEGO-X and the BIC. The time resolution and power consumption requirements differ between the two systems, with AMEGO-X targeting approximately 1  $\mu$ s and below 1.5 mW/cm<sup>2</sup>, while the BIC requires about 20 ns and around 2 mW/cm<sup>2</sup>. In addition, common goals for both applications include achieving an energy resolution better than 10% at 122 keV (FWHM), a target dynamic range covering

25–700 keV, and operating in the fully depleted region to maximize charge collection.

AstroPix\_v3, the first full-scale chip (1.87 cm  $\times$  1.96 cm), has been extensively evaluated for use in both the BIC imaging layers and NASA-led gamma-ray telescopes. AstroPix\_v3 comprises a 35  $\times$  35 pixel matrix with a pixel pitch of 500  $\mu$ m. Each pixel contains a 300  $\times$  300  $\mu$ m<sup>2</sup> high-voltage deep n-well (DNW), which forms a depletion region at the DNW/p-substrate junction under reverse bias. CMOS readout circuitry including a charge amplifier, CR-RC shaper, and comparator, is integrated within each DNW. AstroPix\_v3 was fabricated using TSI Semiconductors’ 180 nm process, with a substrate resistivity of 200–400  $\Omega$ ·cm and thickness of 725  $\mu$ m. Further details can be found in [15].

The design incorporates row and column hit buffers, where each pixel in a single row or column is OR’ed together, effectively resulting in a mock strip detector readout. The chip operates with a 2.5 MHz clock for a time of arrival (ToA) with an 8 bit counter and up to 200 MHz clock for Time-over-Threshold (ToT) measurement with a 12 bit counter. Each hit in a row (resp. column) generates a data packet containing the chip ID, the row (resp. column) number, the ToA, and the ToT.

AstroPix\_v3 employs self-triggering at the pixel level and streaming readout, allowing each pixel to autonomously record hits above threshold. The recorded hit information is matched using row and column data to identify individual hit pixels during the pre-analysis stage, based on the following criteria: (1) the ToA difference is less than 2 clock cycles, and (2) the relative ToT difference, defined as  $(|ToT_{column} - ToT_{row}|)/ToT_{column}$  is required to be below 10%.

### 2.2. Beam test preparation and calibration

As shown in Figure 1, the AstroPix test setup consists of a customized GEneric Configuration and COntrol (GECCO [18]) data acquisition system, a Nexys Video board equipped with an Xilinx Artix-7 FPGA, and a carrier board used to integrate the chips into the GECCO system. Bond pads on a single AstroPix\_v3 chip, located along the lower edge of the chip’s digital periphery, were directly wire-bonded to a rigid carrier PCB for electrical connection and communication via an SPI interface. A bias voltage of -150 V was supplied using a DT5533EN desktop high-voltage power supply module from CAEN Technologies. Analog (VDDA) and digital (VDDDD) supply voltages of 1.8 V, along with a 2.7 V GECCO power voltage, were provided by an HMP404 power supply (Rohde&Schwarz) to power the AstroPix readout circuitry and the FPGA logic, respectively.

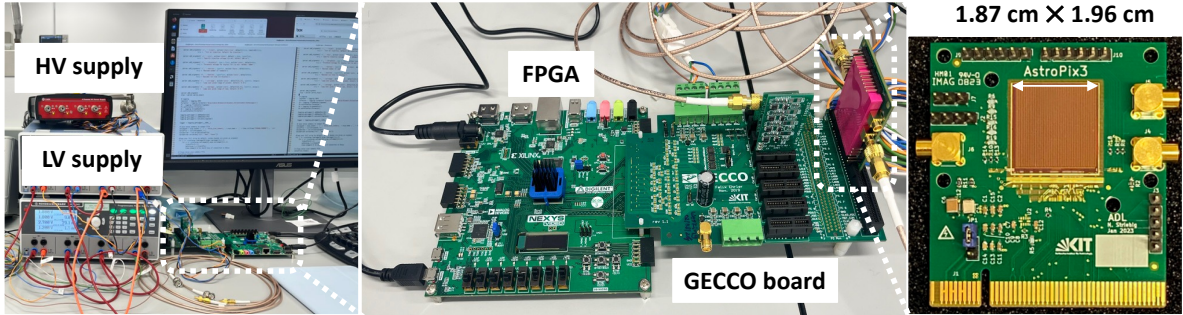


Figure 1: Bench test setup with AstroPix\_v3 single chip.

In preparation for the beam test, noise measurement and radiation source tests were conducted on the bench setup to prepare the experimental configuration. Only one pixel was found to exceed a dark count rate of 2 Hz at 200 mV threshold, as can be seen in Figure 2. The first three columns were excluded because they use a different comparator design, which results in higher noise due to greater amplification. At this threshold, 99.9% of active pixels was achieved.

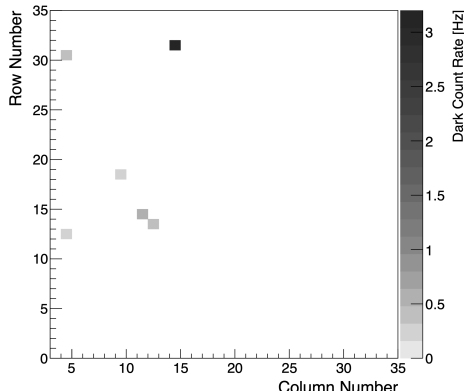


Figure 2: Noise map obtained at a 200 mV threshold, presenting the dark count rate across the pixel array.

The source test was performed using  $^{241}\text{Am}$  and  $^{133}\text{Ba}$  sources to obtain per-pixel energy calibration curves. The ToT distribution from gamma rays of 59.5 keV from  $^{241}\text{Am}$  and 31 keV and 81 keV from  $^{133}\text{Ba}$  were measured per pixel, providing three calibration points. These calibration points are sufficient to convert the measured ToT value into energy, as the deposited MIP energy is expected to lie between 31 keV and 59.5 keV based on the  $^{90}\text{Sr}$  energy measurements.

Figure 3 shows example ToT spectra for one pixel of  $^{241}\text{Am}$  and  $^{133}\text{Ba}$  measurements, where the 31 keV, 59.5 keV, and 81 keV photopeaks are clearly visible and

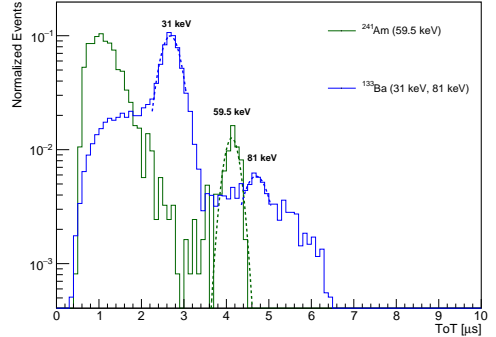


Figure 3: One example of the single-pixel ToT spectra from the  $^{241}\text{Am}$  and  $^{133}\text{Ba}$  measurements is shown. The photopeaks are identified and fitted with Gaussian functions. The green and blue lines correspond to the  $^{241}\text{Am}$  and  $^{133}\text{Ba}$  spectra, respectively, and the dotted lines indicate the fitted Gaussian functions.

fitted with Gaussian functions. Pixels with low statistics or without a visible photopeak were excluded from the calibration. Clear photopeaks of 31 keV, 59.5 keV, and 81 keV were observed in 1,101 pixels (98.3%), 859 pixels (76.7%), and 816 pixels (72.9%), respectively, out of the 1,120 pixels under test. Among these, 683 pixels (61.0%) had clear photopeaks at all three gamma energies and were interpolated using a second-order polynomial, as shown in Figure 4.

The top panels of Figure 4 show the distributions of the centroids obtained from Gaussian fits to the ToT spectra across all selected pixels for each energy point, illustrating pixel-to-pixel variation. Central intervals, presented as 68% in green and 95% in yellow, are overlaid on all calibration curves to indicate the spread of pixel responses.

Compared with the previous study in Ref. [9], 89.6% of the pixels were successfully calibrated using a bias voltage of  $-350$  V, the number of calibrated pixels in this

work is lower. This difference can be mainly attributed to the lower applied bias voltage ( $-150$  V compared to  $-350$  V).

In the previous study [9], an empirical function ( $ToT = ax + b[1 - e^{-x/c}] + d$ , the combination of linear and exponential decay terms) was used to fit from 22.2 keV to 122.1 keV to best match the measured non-linear response of the chip. However, the empirical function could not be applied in this work, as only three data points are available and the number of fit parameters exceeds the number of data points. To assess suitable alternatives, an injection study was performed. AstroPix provides a direct voltage injection feature spanning 100–800 mV, which scales to an equivalent input charge through a response that is not yet fully characterized and therefore requires measurement and calibration. Although this study does not aim to establish an absolute charge calibration, it is sufficient to evaluate and compare two different fitting functions relating injection voltage to ToT.

The top plot of Figure 5 shows example ToT spectra from a representative pixel for injection voltages between 100 mV and 300 mV in 25 mV steps, with all ToT distributions fit using a Gaussian function. This voltage range was chosen because it spans the ToT values corresponding to the 31 keV, 59.5 keV, and 81 keV photopeaks observed in the same pixel. The bottom plot of Figure 5 presents example fits of the ToT value as a function of the injection voltage using two functional forms: the empirical function and a second-degree polynomial. The red solid line and blue dotted line represent the two fits, respectively. Both functions provide consistent results within the ToT range relevant for the 120 GeV proton measurement and the gamma-ray photopeaks. Therefore, a second-degree polynomial function is used as the calibration function in this work.

### 2.3. Beam Test at FTBF

The beam test was conducted at the Fermilab Test Beam Facility (FTBF) in June 2024 using a 120 GeV proton beam. This measurement was part of the same experimental campaign described in [19]. The AstroPix sensor was installed at the MTest beam line in the 6.2A enclosure [10], together with the Pb/SciFi prototype calorimeter.

As shown in Figure 6, the AstroPix sensor was aligned with the geometric center of the beamline using the FTBF laser positioning system. The sensor was oriented with its surface perpendicular to the beam axis and positioned approximately 2 cm upstream of the calorimeter face. Since the multiwire proportional

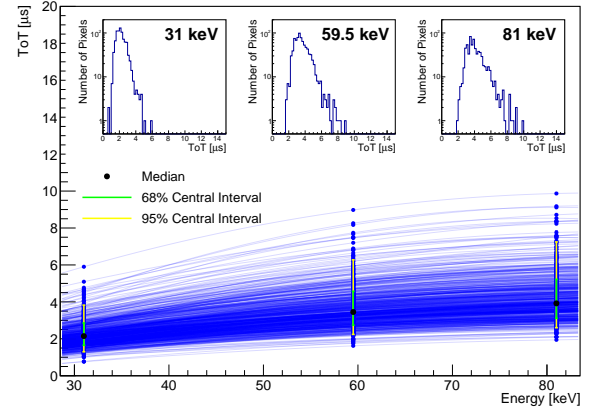


Figure 4: Calibration curves for all selected pixels of a single AstroPix\_v3 chip. Blue lines show fits with the second-degree polynomial function to the mean ToT values extracted from Gaussian fits to the ToT distributions at three gamma energies (31, 59.5, and 81 keV). The upper panels display the distributions of the mean ToT values across pixels for each energy, illustrating pixel-to-pixel variations. The green and yellow bands indicate the 68% and 95% central intervals, respectively.

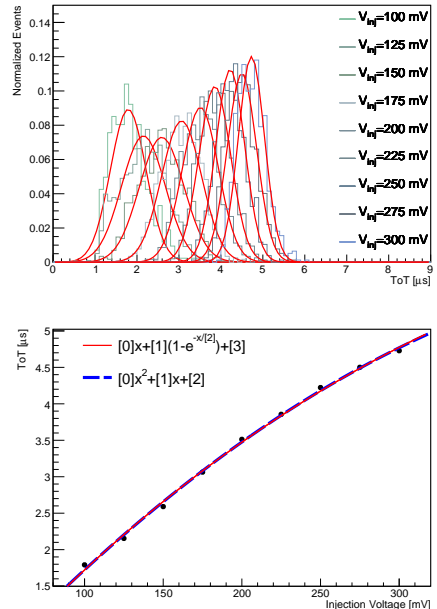


Figure 5: (Top) Example ToT spectra for injection voltages from 100 mV to 300 mV. All ToT distributions are fitted with a Gaussian function. (Bottom) Example fitting results for ToT value as a function of injection voltages using two fit functions: an empirical function (red line) and a second-degree polynomial function (blue dotted line).

chambers typically used for tracking at FTBF were unavailable during this beam period, the AstroPix sensor was employed not only for its primary response stud-

ies but also to provide the beam profile needed for the calorimeter study.

The MTest beamline is capable of delivering protons, muons, and mixed beams of electrons and pions, depending on the configuration of targets, absorbers, and collimators. For this beam test, a 120 GeV primary proton beam, directly extracted from the main injector, was used for AstroPix testing. The beam consists of 100% protons and can be operated at the highest intensity of up to 500,000 particles per spill, with a spot size confined within 6 mm [20]. During the AstroPix test run, the proton beam was delivered in 4.2 s-long spills every minute with about 55,000 particles per spill, resulting in a delivered particle rate of around 13 kHz within each spill.

### 3. Results

#### 3.1. Beam Profile

Figure 7 presents the two-dimensional hit maps of the 120 GeV proton beam for three consecutive 12-hour overnight data-taking runs. The maps represent the number of matched hits in the column–row coordinates of the AstroPix sensor. The sensor surface was oriented perpendicular to the beam axis, so the column and row directions directly correspond to the transverse  $x$ - and  $y$ -directions of the incident beam. To quantify the beam profile, each two-dimensional map was projected onto the column and row axes. By multiplying the column and row indices by the pixel pitch of 500  $\mu\text{m}$ , the projections were converted into physical  $x$ - and  $y$ -coordinate histograms of the number of matched hits. Gaussian functions were fitted to these one-dimensional distributions to extract the beam widths along each axis.

As shown in Figure 8, the extracted beam profiles, obtained from Gaussian fits in  $x$  and  $y$ , were measured to be  $\sigma_x \times \sigma_y = 5.7 \text{ mm} \times 4.4 \text{ mm}$ ,  $4.3 \text{ mm} \times 3.5 \text{ mm}$ , and  $4.3 \text{ mm} \times 3.9 \text{ mm}$  for the three runs, respectively. As mentioned in Section 2.3, in the absence of MWPC-based tracking, the extracted beam profiles could not be directly compared with an independent reference measurement [19]. However, the measured beam widths are consistent with the expected FTBF beam conditions, which specify a proton beam spot size confined within approximately 6 mm, as described in the previous section.

#### 3.2. Energy Measurement

In the 120 GeV proton data analysis, only pixels with more than 1,000 matched hits were used to ensure sufficient statistics for each run. These pixels are predom-

inantly located in the beam center region. For each selected pixel, the ToT distribution was fitted with a Landau function convoluted with a Gaussian function, and the Most Probable Value (MPV) was extracted from the fit. Figure 9 shows a representative two-dimensional hit map and the corresponding fitted ToT distributions for a  $2 \times 2$  pixel region at the beam center, along with the associated fit parameter values.

During the first overnight period, the beam intensity was increased from approximately 55,000 particles per spill to 20–30 million particles per spill, exposing the sensor to this condition for about ten minutes. Under this unexpectedly high beam-rate condition, the pixel dead time increased, the hit rate saturated, and substantially more data loss occurred compared with the other stable runs. Although the ToT spectrum for each pixel can still be well described by a Landau function convoluted with a Gaussian function, the first overnight run was excluded from the energy analysis.

The two other stable runs had 237 and 402 pixels with more than one thousand matched hits, respectively. The ToTs of these pixels were fitted using a Landau function convoluted with a Gaussian function, from which the corresponding MPV values were extracted. After applying the calibrated curves, which are available for 61% of the pixels, the MPV ToT values from 153 and 253 pixels were converted to deposited energy. Figure 10 shows the resulting MPVs from these pixels at the beam center for two runs plotted on the calibration curve. Because both runs had an overlap of 97 pixels, the figure presents calibration results for a total of 406 pixels, all of which are located in rows 21 and below.

All MPV points fall within the energy range between 31 keV and 59.5 keV, as expected. The central intervals of the measured MIP energy, corresponding to 68% (green) and 95% (yellow) levels, are also overlaid. The upper panels of the figure show the ToT and energy distributions of the measured 120 GeV protons. The ToT distribution shape for 120 GeV protons exhibits a pixel-to-pixel variation comparable to those observed for 31, 59.5, and 81 keV calibration points, as shown in the left subpanel of Figure 4, while the corresponding energy distribution follows a Gaussian shape, as illustrated in the right subpanel of Figure 10.

Figure 11 shows the distribution of the pixel-by-pixel MPV energies obtained from the measured 120 GeV proton data, which is well described by a Gaussian distribution. Each entry corresponds to the MPV extracted from an individual pixel. The average MPV across all pixels at the beam center is  $35.4 \pm 1.3 \text{ keV}$ , which are taken from mean and 1 sigma values in Figure 11. It corresponds to an effective depletion depth of  $133 \pm 5 \mu\text{m}$

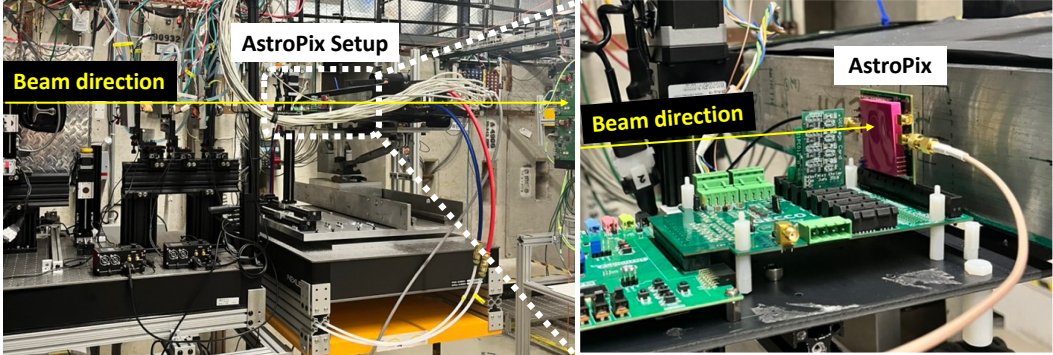


Figure 6: FBTF experimental setup with AstroPix\_v3 single chip.

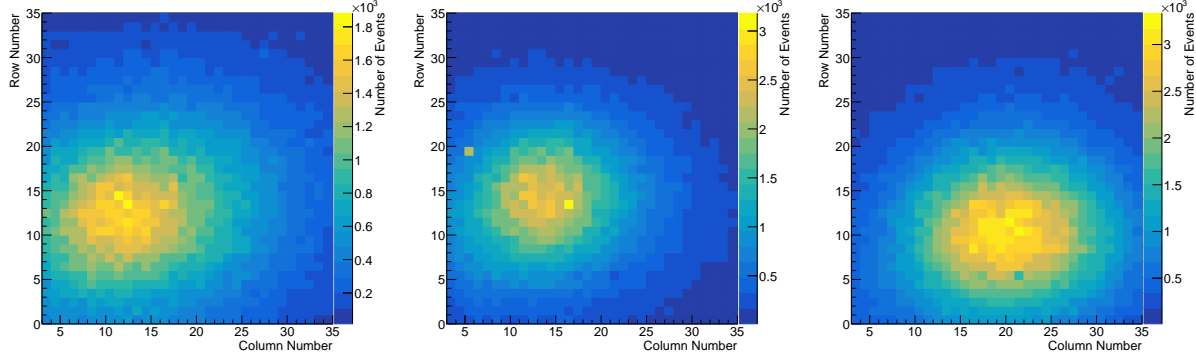


Figure 7: Two-dimensional hit maps of 120 GeV protons for each run. Each map displays the number of matched hits in column–row coordinates of the AstroPix sensor.

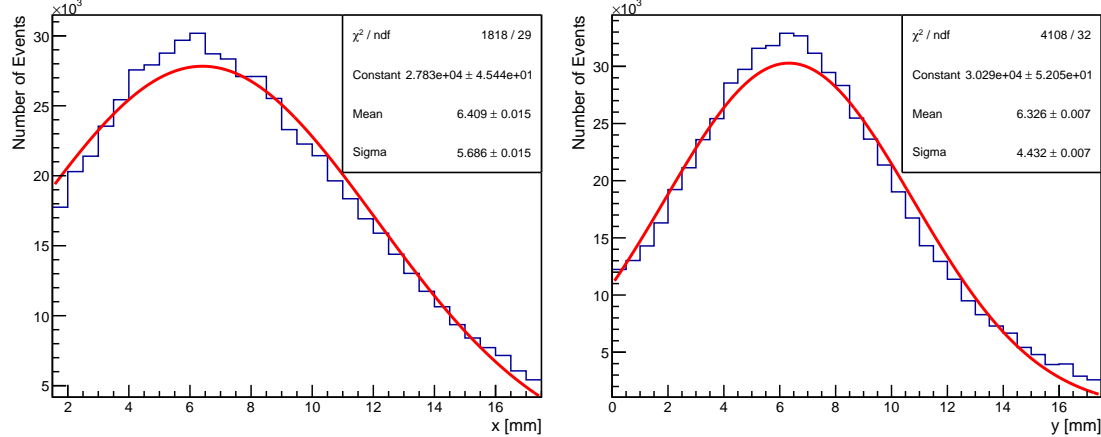


Figure 8: Example beam profile of the first run in the horizontal (left) and vertical (right) directions, obtained by projecting the two-dimensional hit map onto the respective axes. Each histogram is fitted with a Gaussian function and the fit parameters are reported in the legend.

as derived from the most probable energy loss calculation for 120 GeV protons in silicon [21, 22].

To evaluate systematic uncertainties, four sources are

considered. The first source arises from the uncertainty in the MPV extracted from a Landau function convoluted with a Gaussian function, fitted independently for

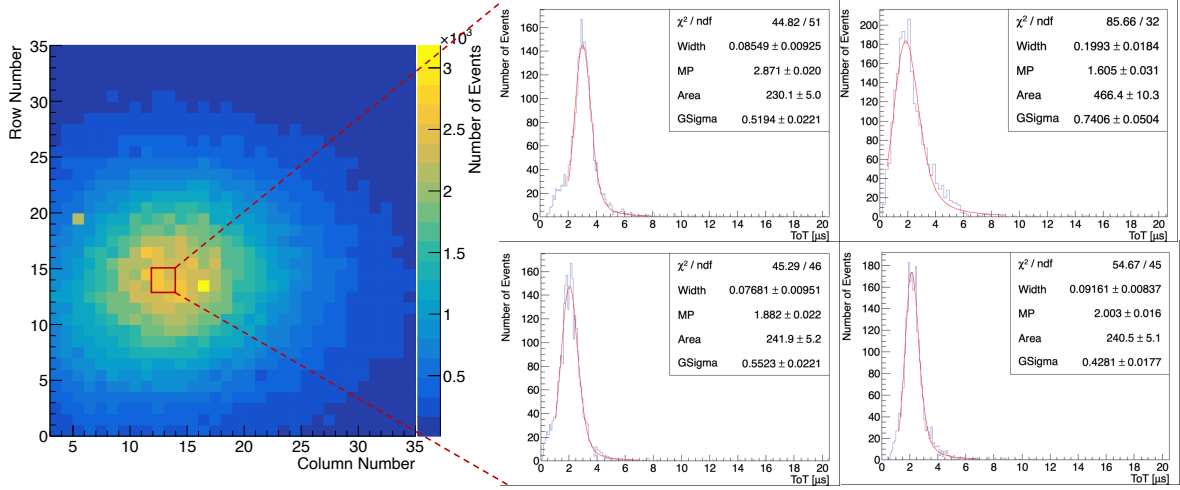


Figure 9: (Left) Example hit map of 120 GeV proton run. (Right) Example fit ToT distributions for  $2 \times 2$  pixels at the beam center. All spectra have been fitted with a Landau function convoluted with a Gaussian function, and the fit parameters are presented in the legend.

each pixel. The uncertainty of the MPV fit, propagated to the final calibrated energy value, is conservatively taken to be 2%.

The second source accounts for the uncertainty in the calibration curve parameters for each pixel. A systematic uncertainty of 1% is assigned.

As a third source, run-by-run fluctuations are evaluated using 97 pixels that overlap between two independent runs. For each pixel, the relative difference in the extracted energy between the two runs is calculated, and the resulting distribution is consistent with a Gaussian distribution. The  $1\sigma$  of the relative energy difference distribution is assigned as a systematic uncertainty of 3%.

The momentum spread of the 120 GeV proton beam is negligible at the level of  $\Delta p/p \sim 2\%$ , as reported in the FTBF documentation [20]. This corresponds to a variation in  $\beta\gamma$  from approximately 125 to 130, which results in no observable change in the most probable energy loss in silicon over this range.

The total systematic uncertainty is therefore obtained to be 3.7%, obtained as the quadrature sum of all sources. Including the systematic uncertainty in quadrature, the measured MPV of the MIP energy is  $35.4 \pm 1.8$  keV, corresponding to a depletion depth of  $133 \pm 6 \mu\text{m}$ .

Figure 11 also indicates a relative pixel-to-pixel variation ( $\sigma/\text{mean}$ ) of 3.9%. This variation predominantly reflects differences in the effective depletion depth, which may be attributed to process-induced defects, wafer-scale inhomogeneities, and local pixel-level bias voltage variations.

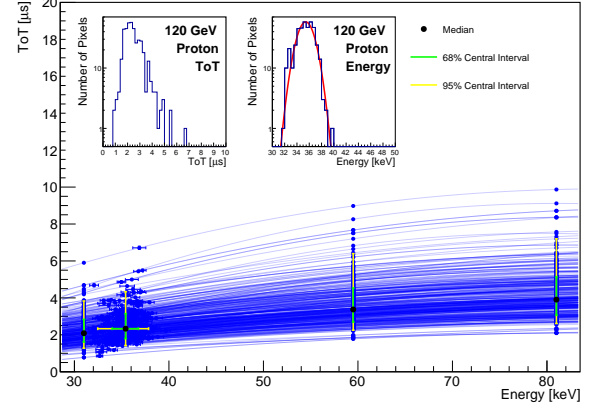


Figure 10: Calibration curves for all selected pixels as a function of energy, including proton measurement results. The upper subplots in each plot show the ToT and energy distributions of the measured 120 GeV protons, respectively.

#### 4. Conclusions & Outlook

AstroPix\_v3 was tested with the 120 GeV proton beam at the Fermilab Test Beam Facility for R&D purposes to study its MIP signal response and to measure the deposited energy and the corresponding effective depletion depth. The ToT distributions from the 120 GeV protons were well described with a Landau function convoluted with a Gaussian function, from which the MPV for MIP signals was extracted on a pixel-by-pixel basis. The average MPV of MIPs across all pixels at the beam center for each run was measured to be 35.4 keV, corresponding to an effective depletion depth of  $133 \pm 5 \mu\text{m}$ . The MIP energy deposition lies well within

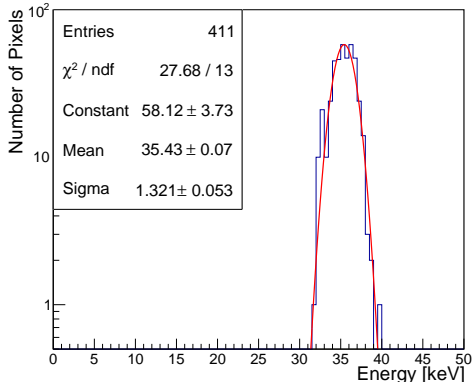


Figure 11: Distribution of the pixel-by-pixel MPV energy obtained from the measured 120 GeV proton data. Each entry corresponds to the MPV extracted from an individual pixel. The red line and the statistics box indicate the Gaussian fit to the distribution.

the AstroPix\_v3 dynamic range of 25–200 keV, demonstrating the suitability of the sensor for MIP detection and energy-deposition measurements. A relative pixel-to-pixel variation of 3.9% was observed in the measured energy deposition of 120 GeV protons, reflecting a corresponding variation in the effective depletion depth across the sensor and indicating excellent uniformity. The extracted depletion depth provides valuable input for detailed detector simulations, enabling more realistic modeling of energy deposition for simulations relevant to space missions as well as future ePIC studies.

Although AstroPix\_v3 is not the final design for the Barrel Imaging Calorimeter (BIC) in the ePIC experiment at the EIC, it plays a critical role in ongoing performance validation and system-integration studies. The current R&D has progressed to multi-layer, daisy-chained multi-chip operation tests, representing a key step toward the full imaging layer implementation. Initial engineering tests were performed with four- and nine-chip prototype modules to validate inter-chip communication, synchronization, and mechanical integration. These prototypes share the same dimensions as the final design and have successfully demonstrated the proof of principle for the nine-chip module PCB mockup, thereby validating its role as the fundamental unit of the BIC imaging layer [23]. In parallel, for space-mission applications, the AstroPix\_v3 quad-chip module is being actively tested and characterized. Ongoing development continues with AstroPix\_v4 [16, 17], which features individual pixel readout and pixel-by-pixel threshold control, implements the design in a smaller format, and is currently under

testing. AstroPix\_v5, designed to achieve a fully depleted region and a dynamic range covering 25–700 keV, is currently under fabrication, and AstroPix\_v6 is being developed as the production version intended for the BIC imaging layer.

## Acknowledgments

Development of AstroPix is funded through the following NASA programs: 18-APRA18-0084 and 20-RTF20-0003. This document was prepared by the members of the Barrel Imaging Calorimeter (BIC) Detector Subsystem Collaboration (DSC) of the ePIC Collaboration using the resources of the Fermi National Accelerator Laboratory (Fermilab), a U.S. Department of Energy, Office of Science, Office of High Energy Physics HEP User Facility. Fermilab is managed by Fermi-Forward Discovery Group, LLC, acting under Contract No. 89243024CSC000002. The material is based upon work partially supported by the U.S. Department of Energy, Office of Science, Office of Nuclear Physics and Laboratory Directed Research and Development (LDRD) funding from Argonne National Laboratory, provided by the Director, Office of Science, of the U.S. Department of Energy under Contract No. DE-AC02-06CH11357; the Electron-Ion Collider Project R&D Funds for the eRD115 Project. We also acknowledge the invaluable support of the FTBF staff, whose expertise and dedication greatly facilitated the execution of our test beam experiments.

## References

- [1] R. Caputo, M. Ajello, C. A. Kierans, J. S. Perkins, J. L. Racusin, L. Baldini, M. G. Baring, E. Bissaldi, E. Burns, N. Cannady, E. Charles, R. M. C. da Silva, K. Fang, H. Fleischhacker, C. Fryer, Y. Fukazawa, J. E. Grove, D. Hartmann, E. J. Howell, M. Jadhav, C. M. Karwin, D. Kocevski, N. Kurahashi, L. Latronico, T. R. Lewis, R. Leys, A. Lien, L. Marcotulli, I. Martinez-Castellanos, M. N. Mazziotta, J. McEnery, J. Metcalfe, K. Murase, M. Negro, L. Parker, B. Phlips, C. Prescod-Weinstein, S. Razzaque, P. S. Shawhan, Y. Sheng, T. A. Shutt, D. Shy, C. Sleator, A. L. Steinhebel, N. Striebig, Y. Suda, D. Tak, H. Tajima, J. Valverde, T. M. Venter, Z. Wadiasingh, R. S. Woolf, E. A. Wulf, H. Zhang, A. Zoglauer, All-sky Medium Energy Gamma-ray Observatory eXplorer mission concept, *Journal of Astronomical Telescopes*,

Instruments, and Systems 8 (4) (2022) 044003. doi:10.1117/1.JATIS.8.4.044003. URL <https://doi.org/10.1117/1.JATIS.8.4.044003>

[2] W. B. Atwood, A. A. Abdo, M. Ackermann, W. Althouse, B. Anderson, M. Axelsson, L. Baldini, J. Ballet, D. L. Band, G. Barbiellini, et al., The large area telescope on the fermi gamma-ray space telescope mission, *The Astrophysical Journal* 697 (2) (2009) 1071–1102. doi:10.1088/0004-637X/697/2/1071.

[3] R. Caputo, C. Kierans, N. Cannady, A. Falcone, Y. Fukazawa, M. Jadhav, M. Kerr, N. Kirschner, K. Kumar, A. Lavorin, R. Leys, J. McEnery, J. Metcalfe, Z. Metzler, N. Miller, J. Mitchell, L. Parker, I. Peric, J. Perkins, B. Phlips, J. Racusin, M. Sasaki, K. N. Segal, D. Shy, A. L. Steinhebel, N. Striebig, Y. Suda, H. Tajima, J. Valverde, D. P. Violette, R. Woolf, A. Zoglauer, ComPair-2: a next-generation medium-energy gamma-ray telescope prototype, in: J.-W. A. den Herder, S. Nikzad, K. Nakazawa (Eds.), *Space Telescopes and Instrumentation 2024: Ultraviolet to Gamma Ray*, Vol. 13093, International Society for Optics and Photonics, SPIE, 2024, p. 130932L. doi:10.1117/12.3017619. URL <https://doi.org/10.1117/12.3017619>

[4] D. P. Violette, A. L. Steinhebel, A. Roy, R. Boggs, R. Caputo, D. Durachka, Y. Fukazawa, M. Hashizume, S. Hesh, M. Jadhav, C. Kierans, K. Kumar, S. Kushima, R. Leys, J. Metcalfe, Z. Metzler, N. Nakano, I. Peric, J. Perkins, L. Seo, K.-W. T. Shin, N. Striebig, Y. Suda, H. Tajima, A-STEP: the AstroPix sounding rocket technology demonstration payload, in: *Space Telescopes and Instrumentation 2024: Ultraviolet to Gamma Ray*, Vol. 13093 of *Proceedings of SPIE*, Yokohama, Japan, 2024, p. 1309381, event: SPIE Astronomical Telescopes + Instrumentation 2024. doi:10.1117/12.3020802. URL <https://doi.org/10.1117/12.3020802>

[5] A. Accardi, et al., Electron Ion Collider: The Next QCD Frontier: Understanding the glue that binds us all, *Eur. Phys. J. A* 52 (9) (2016) 268. arXiv:1212.1701, doi:10.1140/epja/i2016-16268-9.

[6] E. National Academies of Sciences, Medicine, An Assessment of U.S.-Based Electron-Ion Collider Science, The National Academies Press, Washington, DC, 2018. doi:10.17226/25171.

[7] R. Abdul Khalek, et al., Science Requirements and Detector Concepts for the Electron-Ion Collider: EIC Yellow Report, *Nucl. Phys. A* 1026 (2022) 122447. arXiv:2103.05419, doi:10.1016/j.nuclphysa.2022.122447.

[8] J. Adam, et al., ATHENA detector proposal — a totally hermetic electron nucleus apparatus proposed for IP6 at the Electron-Ion Collider, *JINST* 17 (10) (2022) P10019. arXiv:2210.09048, doi:10.1088/1748-0221/17/10/P10019.

[9] Y. Suda, R. Caputo, A. L. Steinhebel, N. Striebig, M. Jadhav, Y. Fukazawa, M. Hashizume, C. Kierans, R. Leys, J. Metcalfe, M. Negro, I. Perić, J. S. Perkins, T. Shin, H. Tajima, D. Violette, N. Nakano, Performance evaluation of the high-voltage CMOS active pixel sensor Astropix for gamma-ray space telescopes, *Nuclear Instruments and Methods in Physics Research Section A: Accelerators, Spectrometers, Detectors and Associated Equipment* 1068 (2024) 169762. doi:<https://doi.org/10.1016/j.nima.2024.169762>.

[10] Fermilab Beam Test Facility, Beam Overview, <https://ftbf.fnal.gov/beam-overview/>, accessed: 2026-02-04.

[11] I. Perić, A novel monolithic pixelated particle detector implemented in high-voltage CMOS technology, *Nuclear Instruments and Methods in Physics Research Section A: Accelerators, Spectrometers, Detectors and Associated Equipment* 582 (3) (2007) 876–885, vERTEX 2006. doi:<https://doi.org/10.1016/j.nima.2007.07.115>.

[12] I. Brewer, M. Negro, N. Striebig, C. Kierans, R. Caputo, R. Leys, I. Peric, H. Fleischhacker, J. Metcalfe, J. Perkins, Developing the future of gamma-ray astrophysics with monolithic silicon pixels, *Nucl. Instrum. Meth. A* 1019 (2021) 165795. arXiv:2109.13409, doi:10.1016/j.nima.2021.165795.

[13] A. L. Steinhebel, H. Fleischhacker, N. Striebig, M. Jadhav, Y. Suda, R. Luz, C. Kierans, R. Caputo, H. Tajima, R. Leys, I. Peric, J. Metcalfe, J. S. Perkins, AstroPix: novel monolithic active pixel silicon sensors for future gamma-ray telescopes, *Proc. SPIE Int. Soc. Opt. Eng.*

12181 (2022) 121816Y. arXiv:2209.02631, doi:10.11117/12.2630405.

[14] A. L Steinhebel, R. Caputo, H. Fleischhack, N. Striebig, M. Jadhav, Y. Suda, R. Luz, D. Violette, C. Kierans, H. Tajima, Y. Fukazawa, R. Leys, I. Peric, J. Metcalfe, M. Negro, J. S Perkins, AstroPix: CMOS pixels in space, in: Proceedings of 10th International Workshop on Semiconductor Pixel Detectors for Particles and Imaging — PoS(Pixel2022), Vol. 420, 2023, p. 020. doi:10.22323/1.420.0020.

[15] A. L. Steinhebel, D. P. Violette, R. Caputo, A. Affolder, A. Bauman, C. Chinatti, A. Deshmukh, V. Fadayev, Y. Fukazawa, M. Jadhav, C. Kierans, B. Kim, J. Kim, H. Klest, O. Kroger, K. Kumar, S. Kushima, J.-M. Lauenstein, A. Laviron, R. Leys, F. Martinez-Mckinney, J. Metcalfe, Z. Metzler, J. W. Mitchell, N. Nakano, J. Ott, I. Peric, J. S. Perkins, M. R. Rudin, T. K. Shin, G. Sommer, N. Striebig, Y. Suda, H. Tajima, J. Valverde, M. Zurek, AstroPix: A Pixelated HVCMOS Sensor for Space-Based Gamma-Ray Measurement, Nuclear Instruments and Methods in Physics Research Section A: Accelerators, Spectrometers, Detectors and Associated Equipment 1083 (2026) 171021. doi:10.1016/j.nima.2025.171021. URL <https://doi.org/10.1016/j.nima.2025.171021>

[16] Y. Suda, R. Caputo, D. Violette, G. Sommer, N. Striebig, M. Jadhav, Y. Fukazawa, C. Kierans, R. Leys, J. Metcalfe, N. Nakano, I. Perić, J. S. Perkins, H. Tajima, Evaluation of Gamma-Ray Response of the AstroPix4 HV-CMOS Active Pixel Sensor, Nuclear Instruments and Methods in Physics Research Section A: Accelerators, Spectrometers, Detectors and Associated Equipment 1081 (2026) 170839. doi:10.1016/j.nima.2025.170839. URL <https://doi.org/10.1016/j.nima.2025.170839>

[17] N. Striebig, R. Leys, I. Peric, R. Caputo, A. L. Steinhebel, Y. Suda, Y. Fukazawa, M. Jadhav, D. Violette, C. Kierans, H. Tajima, J. Metcalfe, J. S. Perkins, AstroPix4 — a Novel HV-CMOS Sensor Developed for Space-Based Experiments, Journal of Instrumentation 19 (2024) C04010. doi:10.1088/1748-0221/19/04/C04010. URL <https://doi.org/10.1088/1748-0221/19/04/C04010>

[18] R. Schimassek, Development and characterisation of integrated sensors for particle physics, Ph.D. thesis, Ph. D. thesis, Institute for Data Processing and Electronics, Karlsruhe (2021).

[19] H. Klest, M. Žurek, T. Beattie, M. Jadhav, S. Joosten, M. Kerr, B. Kim, M. Kim, J. Metcalfe, Z. Papandreou, J. Richards, J. Zarling, Evaluation of the response to electrons and pions in the scintillating fiber and lead calorimeter for the future electron-ion collider, Journal of Instrumentation 20 (07) (2025) P07028. doi:10.1088/1748-0221/20/07/P07028. URL <https://doi.org/10.1088/1748-0221/20/07/P07028>

[20] Fermilab Beam Test Facility, MTest Beam Details, <https://ftbf.fnal.gov/mtest-beam-details-2/>, accessed: 2026-02-04.

[21] S. Navas, et al., Review of particle physics, Phys. Rev. D 110 (3) (2024) 030001. doi:10.1103/PhysRevD.110.030001.

[22] H. Bichsel, Straggling in thin silicon detectors, Rev. Mod. Phys. 60 (1988) 663–699. doi:10.1103/RevModPhys.60.663. URL <https://link.aps.org/doi/10.1103/RevModPhys.60.663>

[23] B. Kim, R. Caputo, M. Jadhav, S. Joosten, A. Laviron, R. Leys, J. Metcalfe, N. Striebig, D. Violette, M. Žurek, Performance of the AstroPix Prototype Module for the Barrel Imaging Calorimeter at the ePIC Detector and in Space-Based Payloads (2025). arXiv:2511.05639. URL <https://arxiv.org/abs/2511.05639>